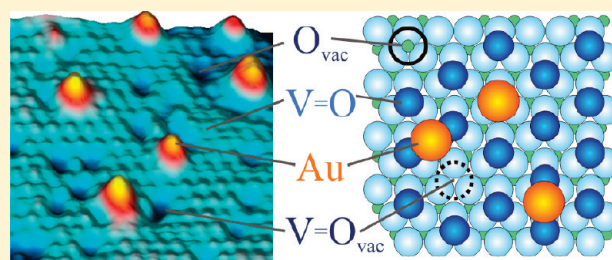


Role of the $V_2O_3(0001)$ Defect Structure in the Adsorption of Au Adatoms

Bing Yang, Xiao Lin, Niklas Nilius,* and Hans-Joachim Freund

Fritz-Haber-Institut der Max-Planck-Gesellschaft, Faradayweg 4-6, D-14195 Berlin, Germany

ABSTRACT: The interaction of Au atoms with point defects in a vanadyl-terminated $V_2O_3(0001)$ film has been investigated with low-temperature scanning tunneling microscopy (STM). For this purpose, oxygen and vanadyl vacancies were introduced into the oxide surface via electron bombardment and characterized with STM topographic imaging and conductance spectroscopy. In addition, water titration experiments have been performed to distinguish the different types of point defects. Oxide films with increasing defect densities have then been prepared to explore the interaction of individual Au atoms with the surface. Up to the highest defect concentration, regular bridge sites in the vanadyl lattice were identified to be the preferred Au adsorption sites. This is in conflict with recent DFT calculations that found Au binding to oxygen vacancies to be much stronger than to regular surface sites. Possible reasons for the discrepancy are discussed in the text.



1. INTRODUCTION

It is general perception that surface defects control the adsorption properties of oxide materials.^{1,2} Their importance is due to the chemical inertness of an ideal oxide surface that reflects the high degree of bond saturation of the metal–oxygen network. In addition, many oxides are characterized by a gap in their electronic structure, which further diminishes their susceptibility to interact with adsorbates. Both properties are neutralized in the vicinity of defects, which either expose unsaturated dangling bonds or induce localized states in the oxide band gap.^{3,4} Defects may therefore provide suitable binding sites for ad-species on the otherwise inert surface.^{1,5} A good understanding of defect properties is also required if one seeks insight into chemical reactions taking place on oxide surfaces. In the most desirable scenario, the knowledge on defects goes down to the atomic level and includes the exploration of adsorption events on single, well-characterized surface sites. Such experiments are indeed feasible with scanning tunneling (STM) and atomic force microscopy (AFM) and have been performed on various adsorbate–oxide systems, for example, for H_2O ,^{6,7} CO ,⁸ and different alcohols on $TiO_2(110)$,⁹ $ZnO(0001)$,¹⁰ and $FeO(111)$.¹¹

The different compounds of vanadium, in particular V_2O_3 and V_2O_5 , have always been in the focus of oxide research.^{12–14} The studies are driven by the importance of vanadia-based systems in heterogeneous catalysis, in particular in oxidation and dehydrogenation reactions. Also, from the academic viewpoint, vanadium oxides are interesting thanks to the large variety of chemical compositions, crystallographic structures, surface terminations, and defect properties they adopt in different environments. Vanadium compounds are therefore ideal model systems to study the influence of surface properties on the adsorption behavior and chemical activity of reducible oxides.

Three well-defined terminations can be produced on the $V_2O_3(0001)$ surface at ultrahigh-vacuum (UHV) conditions.¹² The most stable one is the (1×1) vanadyl termination that spontaneously forms in a broad pressure and temperature range.¹⁵ It contains one $V=O$ group per surface unit cell, bound to a closed-packed, bulk-like O_3 layer. At high oxygen chemical potential, an oxygen-rich $(\sqrt{3} \times \sqrt{3})R30^\circ$ surface develops that exposes none or few $V=O$ groups but an additional V atom in the subsurface layer, according to a layer sequence of $-V_2-O_3-V_3-O_3$.^{15,16} A V-terminated surface, on the other hand, only forms in a highly reducing chemical environment. V-rich surfaces are either produced by depositing extra vanadium¹⁶ or bombarding a $V=O$ -terminated surface with energetic electrons.¹³ The latter process stimulates the cleavage of $V=O$ bonds and leads to desorption of vanadyl oxygen. All three terminations come along with a number of point defects. While $V=O$ and O vacancies are the characteristic defects in the vanadyl-terminated $V_2O_3(0001)$, residual $V=O$ groups and voids in the topmost oxide layer are commonly observed for the O and V termination.¹²

The influence of a particular termination/defect structure on the adsorption properties of $V_2O_3(0001)$ has been investigated with various methods, including thermal desorption (TDS), photoelectron (UPS, XPS), and infrared-absorption spectroscopy as well as STM. A large number of studies were hereby devoted to water.^{16,17} On the $V=O$ - and O-terminated surface, H_2O binds associatively with desorption temperatures below 350 K. In contrast, dissociative adsorption was found for the V

Received: November 10, 2010

Revised: January 7, 2011

Published: February 09, 2011

termination and leads to desorption temperatures below 550 K. Also, isolated O defects, produced by electron bombardment of the vanadyl surface, turned out to be active in water dissociation at 300 K. Similar experiments have been reported for methanol on V_2O_3 and $V_2O_3(0001)$, where again the O defects are responsible for dissociating CH_3OH into a methoxy species and a surface $-OH$ group.¹⁸ The role of V_2O_3 surface defects was also investigated for O_2 , CO, propane, and propene adsorption using TDS and XPS.^{19,20}

Real space experiments using STM have been performed to explore the interaction of methanol and phthalocyanine (MgPc) with defects in the $V_2O_3(0001)$ surface.^{21,22} Whereas methanol exclusively binds to O defects in the $V=O$ termination, the much larger MgPc also attaches to $V=O$ defects by forming van der Waals bonds. In addition, adsorption of single Au atoms has been investigated on a defective vanadyl $V_2O_3(0001)$ at cryogenic temperature (5 K).²³ Surprisingly, the adatoms exhibit only a small affinity to bind to the $V=O$ vacancies and prefer a bridge configuration between two regular $V=O$ groups. This result has been confirmed by DFT calculations, which determined the Au binding energy to $V=O$ defects to be 0.8 eV lower than that to regular $V=O$ bridge sites. Stronger bonds are only formed to O defects in the surface, in good agreement with the results obtained for water and methanol. However, as the initial concentration of O defects is low in well-prepared $V_2O_3(0001)$, the Au adsorption behavior is dominated by regular sites in the oxide surface.

In this STM work, we revisit the Au binding characteristic on vanadyl-terminated $V_2O_3(0001)$ films grown on Au(111). By producing both kinds of defects, $V=O$ and O vacancies, a comparison between defect-mediated and regular adsorption mechanisms becomes possible. Although multiple evidences for the presence of O defects are provided, the theoretically predicted dominance in anchoring the Au atoms could not be observed.²³ We discuss a number of reasons that might be responsible for this discrepancy.

2. EXPERIMENT

All experiments were carried out in a custom-built, UHV STM operated at 5 K.²⁴ While surface imaging is performed at constant-current conditions, conductance spectroscopy (dI/dV) is done with lock-in technique and disabled feedback loop (modulation bias of 10 mV rms). According to the Tersoff–Haman picture, the dI/dV signal is taken as a measure for the local density of states (LDOS) in the sample. The $V_2O_3(0001)$ is prepared as a thin film with 3–5 nm thickness grown on Au(111). For this purpose, V is dosed at 300 K in an O_2 ambience of 5×10^{-7} mbar onto a sputtered/annealed Au(111) surface (atom flux of 0.5 ML/min). Subsequent annealing to 1000 K for 10 min promotes crystallization of the oxide into large (0001)-oriented patches. At the given experimental conditions, the V_2O_3 surface is entirely covered with a (1×1) $V=O$ layer, exhibiting a defect concentration of ~ 3 –5%. On the basis of earlier results,^{12,15,23} those natural defects are assigned to $V=O$ vacancies. Oxygen defects exposing an unsaturated V atom are produced by irradiating the film at 300 K with 100 eV electrons of varying dosages (0.3–5 mC).^{13,18} Low amounts of water are adsorbed at ~ 150 K onto the freshly prepared film, while Au adatoms are deposited from a gold-plated W-filament at 15 K.

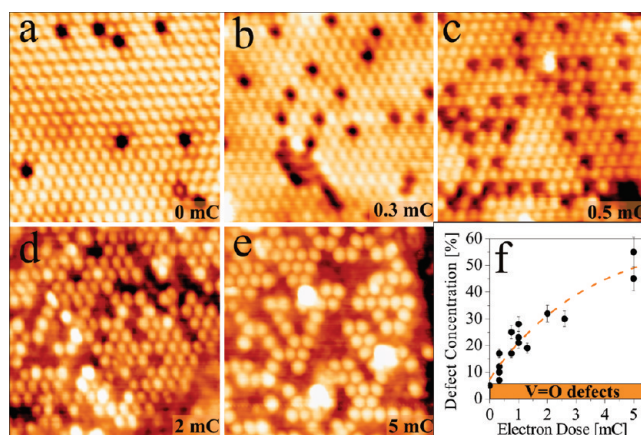


Figure 1. (a–e) STM images of vanadyl-terminated $V_2O_3(0001)$ films on Au(111) irradiated with increasing dosages of 100 eV electrons ($U_s = 0.5$ V, 8.1×8.1 nm²). The depressions are $V=O$ and O defects in the surface, the latter being created by the injected electrons. (f) Evolution of the defect concentration with electron dosage, as determined from 17 independent preparations. The square at the bottom of the diagram marks the intrinsic defect density in as-prepared films.

3. RESULTS AND DISCUSSION

3.1. Vanadyl versus Oxygen Defects. To analyze the role of point defects in vanadyl $V_2O_3(0001)$ on the Au adsorption behavior, it is necessary to distinguish the different defect types first. Unfortunately, a distinction between $V=O$ and O vacancies, being the dominant surface defects, turned out to be difficult as both features have similar topographic and spectroscopic signatures in the STM. In topographic images, they appear as circular depressions of ~ 0.3 Å depth, a number that is rather insensitive to the sample bias. Their dI/dV spectra are governed by the V_2O_3 band gap that opens below the Mott transition at 150 K. In films prepared here, the gap size amounts to 0.4–0.6 eV and slightly depends on the local oxide stoichiometry.²⁵ The strongly rising dI/dV signal outside the gap inhibits the detection of tiny differences in the electronic structure of $V=O$ and O defects, rendering their assignment difficult.

We have therefore employed two indirect methods to quantify the number of $V=O$ versus O vacancies in differently prepared V_2O_3 films. The first approach is based on simply counting the defects that are created by exposing the films to a defined electron dosage. A corresponding STM image series is shown in Figure 1. Image (a) only displays $V=O$ vacancies, as the sample was thermally treated but not irradiated with electrons. From such measurements, the average $V=O$ defect concentration is determined to 3–5% in the as-prepared film. After electron irradiation, more and more point defects appear in the vanadyl-terminated surface and finally merge to large $V=O$ free patches (Figure 1e). The majority of those defects are assigned to O vacancies, although removal of the remaining V atoms becomes increasingly probable at high electron exposure. Panel (f) displays the evolution of the defect density as a function of electron dose. While the concentration increases linearly at small exposure,²¹ a saturation effect sets in on heavily reduced samples.

The second method uses the possibility to titrate the O defects with H_2O molecules. As demonstrated in earlier work,^{16,17} O vacancies are more susceptible to stabilize water than are $V=O$ defects. The number of attached molecules with respect to uncovered defect sites thus provides a measure of the O to

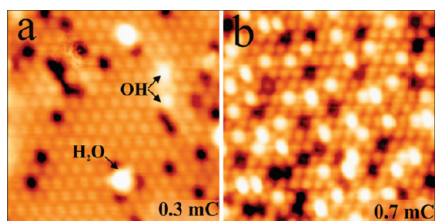


Figure 2. (a,b) Weak and medium-reduced vanadyl $V_2O_3(0001)$ films exposed to small amounts of water at 150 K ($U_s = -0.5$ V, 8.1×8.1 nm²). Water preferentially binds to surface O defects as intact molecule but sometimes dissociates into two $-OH$ groups. At saturation coverage, the numbers of protruding molecules and depressions in the surface provide a measure for the ratio of O versus $V=O$ defects in the film.

$V=O$ defect ratio. The STM image in Figure 2a has been taken after dosing tiny amounts of water onto a mildly reduced sample. At the deposition temperature of 150 K, many intact H_2O molecules and only a few OH groups are observed. The two species are distinguished via their different apparent heights (H_2O , 0.7 Å and OH , 0.2 Å) but both sit in on-top positions of the $V=O$ lattice. As no adsorption is revealed prior to electron irradiation, we assign the binding sites to O defects in the film in agreement with earlier studies.^{16,17} The fact that a large portion of the molecules binds associatively suggests that water is at the verge of dissociation at 150 K dosing temperature. At 300 K, dissociation clearly dominates the H_2O interaction with the O defects.¹⁷ At higher exposure, all O defects are expected to bind a water molecule, leaving only the $V=O$ vacancies as visible holes in the oxide surface. Consequently, the ratio of both defect types can be determined from the number of protrusions (H_2O species) versus depressions ($V=O$ defects) in the STM images. The small number of dissociated molecules is neglected in this approximation. Corresponding measurements have been performed on medium-reduced V_2O_3 films (electron dosage: 0.7 mC, Figure 2b). In the displayed surface region, 25 depressions (7% of all $V=O$ groups) appear together with 52 protrusions (18% of all $V=O$ groups), yielding a $V=O$ to O defect ratio of 1–2. This value matches the approximation obtained from defect-counting on similar films (Figure 1f), demonstrating the suitability of water titration to identify the different point defects in the vanadyl-terminated surface.

Two additional experiments prove the existence of O defects in the electron-bombarded vanadia surface. The first one reveals spontaneous healing of a point defect, being observed in long series of STM images (Figure 3). In panel (a), a surface defect is discernible at the circled position, which seems to be healed in panel (b). Spontaneous filling of a vacancy is only plausible for an O defect, as the required oxygen might be supplied from the rest gas or the STM tip. In contrast, annihilation of a $V=O$ defect appears unlikely, as no V atoms are available on the surface at the experimental conditions. It is interesting to note that simultaneously recorded dI/dV images exhibit a clear contrast between the O defect that fills up later and adjacent defect sites. Apparently, O and $V=O$ vacancies exhibit different electronic properties that can be detected at particular tip and bias conditions (0.5 V) and exploited to distinguish the two species. The enhanced dI/dV signal at 0.5 V does, however, not provide a reliable fingerprint to identify the O defects with STM spectroscopy. A second experiment uses the possibility to dissociate water molecules with the electron beam from the STM tip (Figure 3c). In most cases, no depression remains visible after the stimulated

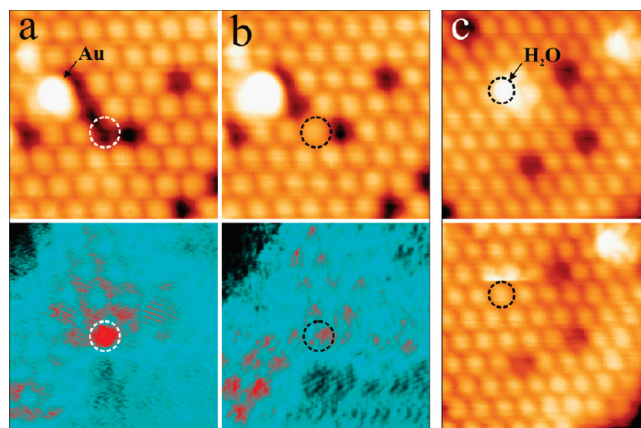


Figure 3. (a,b) Subsequently taken STM images of a weakly reduced $V_2O_3(0001)$ film ($U_s = 0.5$ V, 3.5×3.5 nm²). Upon scanning, the defect marked by the circle heals spontaneously, indicating its nature as an O defect. Also, in the associated dI/dV images shown below, this defect appears with different contrast ($U_s = 0.5$ V). The difference in dI/dV intensity is, however, not reproducible enough to assign O and $V=O$ vacancies on the basis of their spectral response. (c) Stimulated dissociation of a water molecule at low sample bias ($U_s = -0.2$ V, 4.3×4.3 nm²). Apparently, the underlying defect disappears upon dissociation, a process that is only feasible for O but not for $V=O$ vacancies.

dissociation, suggesting that the vacancy is healed by the oxygen atom of the H_2O , while the hydrogen desorbs from the surface. Again, annihilation of a $V=O$ defect via water dissociation seems to be unlikely.

The experiments presented so far conclusively demonstrate the presence of both O and $V=O$ defects on a vanadyl-terminated V_2O_3 surface irradiated with electrons. The interaction of these defects with Au atoms will be discussed in the following paragraph.

3.2. Gold Adsorption on Electron-Bombarded V_2O_3 Films. Vanadia films exposed to three different electron dosages (0.3, 0.7, and 3 mC) have been prepared to evaluate the influence of surface defects on the Au adsorption behavior. The defect density was hereby found to increase from 7%, 15%, to 30% of the total number of $V=O$ sites, $\sim 5\%$ of them being natural $V=O$ vacancies (see Figure 1f). A defined number of Au atoms (1×10^{13} cm⁻²) were then deposited onto each sample at 15 K. The adatoms are readily identified as circular protrusions of ~ 1 Å height and ~ 8 Å diameter in the respective STM images (Figure 4a–c). Their binding site with respect to the $V=O$ groups is determined by superimposing the vanadyl lattice onto the adatom position. While adatoms sitting directly on a $V=O$ lattice site are assigned to defect-bound species, as Au does not adsorb on-top of a $V=O$, a position between adjacent vanadyls is indicative for regular binding.²³ Apart from topographic imaging, the Au adsorption behavior was analyzed with STM conductance spectroscopy as well as by desorbing the ad-species with controlled voltage pulses and imaging the hence uncovered surface. A combination of all three methods allows us to unequivocally determine the Au adsorption geometry.

Already on weakly reduced oxide samples, as shown in Figure 4a, different Au binding configurations are discernible. Whereas adatoms 2 and 3 sit in bridge positions between two adjacent $V=O$ groups, the slightly fainter species 1 and 4 occupy top sites on the vanadyl lattice. The remaining features are assigned to small gold aggregates, the internal structure of which

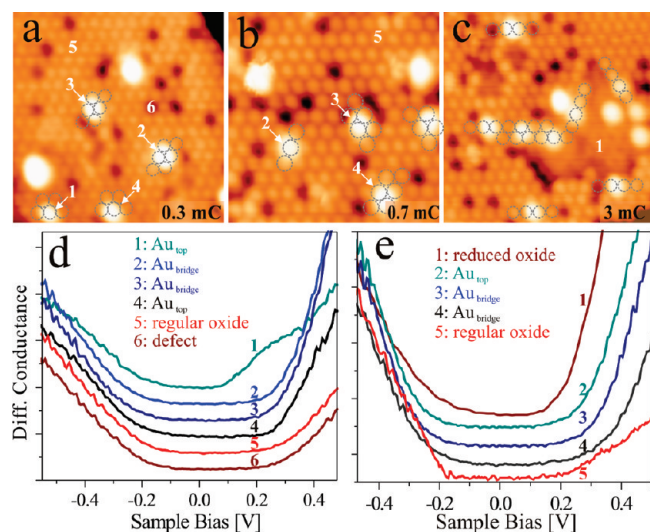


Figure 4. (a–c) STM images of differently reduced $V_2O_3(0001)$ films exposed to a small amount of Au at low temperature ($U_s = -0.5$ V). The image sizes are (a,c) 8.1×8.1 nm² and (b) 6.2×6.2 nm². The adatom binding sites have been determined by overlying the $V=O$ lattice onto each adsorbate. (d) dI/dV spectra taken at the surface positions indicated in panel (a). The spectroscopy set-point was set to -0.5 V. With the exception of spectrum 1 that shows an Au-induced gap state, the dI/dV curves are governed by the low-temperature band gap of V_2O_3 . (e) Similar spectra measured at surface positions in panel (b) (spectra 2–5) and (c) (spectrum 1).

could not be identified with the STM. The different adsorbates are further characterized with the help of their conductance spectra. The dI/dV response of bridge-bonded adatoms (e.g., 2 and 3) corresponds to the one of the bare film that is governed by the band gap at the Fermi level (Figure 4d). Also, 4, occupying a top site, does not exhibit a spectral feature by its own. Only the apparently similar species 1 induces a new state at $+0.3$ V inside the gap region of the oxide, manifesting its different nature.

The interrelation between electronic structure and binding site of individual Au atoms on $V_2O_3(0001)$ has already been analyzed in an earlier study and can now be applied to identify the various surface species.²³ The sole adsorbates with a localized state in the band gap are Au atoms attached to a $V=O$ defect. The gap state corresponds to the Au 6s orbital that remains close to the Fermi level due to the negligible interaction between the adatom and the close-packed O_3 layer below the $V=O$ vacancy. This situation applies to the top-bound species 1 in Figure 4a. Feature 4, on the other hand, is assigned to an atom sitting in an O defect of the vanadyl lattice. In this configuration, the Au 6s orbital strongly interacts with the partly filled 3d levels of the unsaturated V atom in the vacancy. The resulting mixed states shift out of the gap region, where they overlap with the vanadia bulk bands and become undetectable with dI/dV spectroscopy. A similar situation occurs for regular-bound Au atoms located between two $V=O$ groups (species 2 and 3). Also here, Au-induced states appear exclusively outside the vanadia band gap due to an effective hybridization with the $V=O$ electronic states. Nonetheless, adatoms on regular and O-defect sites are distinguishable due to their different binding positions with respect to the vanadyl lattice.

On weakly reduced $V_2O_3(0001)$ films, the bridge-bonded Au atoms are identified as majority species that comprise more than 90% of all adsorbates. Although this result is not reflected in

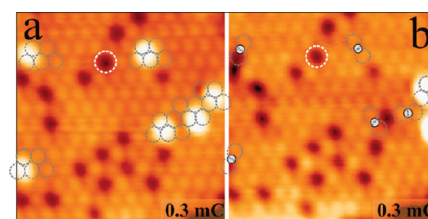


Figure 5. (a) STM image of weakly reduced $V_2O_3(0001)$ exposed to a small amount of Au at low temperature ($U_s = -0.5$ V, 6.2×6.2 nm²). The Au binding sites have been determined by overlying the $V=O$ lattice onto the adatom positions. In all cases, the atoms occupy regular bridge sites in the $V=O$ lattice. (b) Same image after removing the adatoms with 1.0 V pulses. The initial atom positions are marked with small white disks. The broken circle identifies an identical position in (a) and (b) as a guide to the eye. During manipulation, the right-most atom has transformed into a dimer, and a new feature appeared on the right rim of the image.

Figure 4a, being selected to introduce the different Au species, it becomes evident in Figure 5a that has been measured on a similar oxide film (0.3 mC electron dose). All six adatoms in this image sit on regular $V=O$ bridge sites, while the 21 defects remain uncovered. This finding is supported by the associated dI/dV spectra, none of them displaying a localized state in the oxide band gap. Also, after desorbing the adatoms with 1.0 V voltage pulses, no vacancy becomes visible below their original position, indicating a regular adsorption geometry (Figure 5b). It is, however, worth mentioning that defects occasionally occur in direct vicinity of the removed ad-species, as observed for the two left-most adsorbates in Figure 5. This observation suggests that the defects might be surrounded by a barrier that reduces their accessibility for adsorbates. In general, pristine and weakly reduced V_2O_3 films behave identical to what the preferred attachment of Au atoms to the regular $V=O$ bridge sites concerns.²³

Surprisingly, this situation does not change very much with increasing reduction of the oxide surface. In Figure 4b already 15% of the $V=O$ groups are perturbed, still three out of four Au atoms occupy regular bridge sites and only one sits in a defect-related top position. Based on the associated dI/dV spectrum, this adatom occupies an O vacancy (Figure 4e, spectrum 2). Also, the small aggregates in the upper part of the image might be anchored on defect sites; however, their exact binding position cannot be deduced with the STM. The maximum fraction of defect-bound adsorbates is therefore still below 50%, despite the substantial defect concentration in the surface. With increasing electron irradiation, the binding situation of Au becomes even more complex (Figure 4c). The bridge-bonded Au atoms remain the prevalent species in regions where large amounts of vanadyls are still present. A second group of atoms is found along the boundaries between $V=O$ rich and $V=O$ depleted surface patches and mainly occupies on-top positions of the original vanadyl lattice. None of these species exhibit a gap state in their dI/dV spectrum, which indicates an attachment to O defects at the boundary. On the other hand, the number of Au atoms in regions without $V=O$ groups is small, suggesting a low binding strength for gold. This behavior is incompatible with a V-termination of such areas, because the surface vanadium would enable a strong interaction with gold.²³ Apparently, those patches have been reduced even further during electron irradiation and expose already the bulk-like and chemically inert O_3 layer below the $V=O$ groups.¹⁵ As this conclusion is entirely based on the low

concentration of Au species, additional experiments would be required to safely determine the nature of the heavily reduced regions.

In summary, the observed low-temperature adsorption behavior of Au on reduced vanadia films is not governed by defects even if their concentration is as high as 50%. In all samples, adatoms on regular V=O bridge positions are the most abundant species, while top-bound atoms, indicative for a defect-mediated binding, are less common. This finding is in conflict with the results of DFT calculations, which connect the largest Au adsorption potential to O defects with an exposed V atom in the V_2O_3 surface. Possible reasons for this discrepancy are discussed in the next section.

3.3. Discussion. The calculated Au binding strength to regular and defect sites of vanadyl-terminated $V_2O_3(0001)$ evolves from 1.0 eV for V=O vacancies, 1.8 eV for regular V=O bridge sites to 2.0 eV for O vacancies.²³ Only the V-terminated surface that seems not to be present in our experiment has a higher binding potential of 2.3 eV. In thermal equilibrium, the occupancy of the different sites is governed by a Boltzmann distribution according to the binding energy. A first estimation of the Au distribution might be obtained by setting the equilibrium temperature to the Au impingement temperature of ~ 1000 K. In this case, only 0.0005% and 8% of the adatoms should attach to V=O defects and regular V=O bridge sites, respectively, while 91% should occupy O-defect sites. Accounting for the quick thermalization of the incoming adsorbates, the number of Au species bound to O defects should be even larger. This is in clear disagreement with the experimental results that reveal the regular bridge site to be the preferred adsorption position.

The discrepancy between the measured and calculated Au adsorption behavior might be caused by several factors. The most plausible explanation is that kinetic and not thermodynamic aspects control the Au distribution on the oxide surface. More precisely, incoming Au atoms might dissipate their energy too quickly to explore an extended surface region and rather stick close to their impingement site. As long as the vanadyl lattice is more or less intact, those sites are naturally the regular V=O bridge sites, in agreement with the STM data. Quick energy dissipation of adsorbates is rather uncommon for oxide surfaces, given their small density of electronic and phononic modes around the Fermi level. For example, self-assembly processes of Au atoms on alumina, magnesia, and wustite films indicate transient adsorbate mobility on a 10 nm length scale even at 15 K.^{26,27} The short travel lengths anticipated here can be explained with the relatively strong Au binding to the vanadyl-terminated $V_2O_3(0001)$. Also, the large vibrational flexibility of the V=O groups might facilitate energy dissipation and promotes quick thermalization of the incoming adsorbates. Both effects would lead to the kinetically controlled Au adsorption behavior suggested by the experiments. On the other hand, the detection of small Au aggregates on the vanadia surface indicates transient adatom mobility even at 15 K.

Furthermore, although the O defects have a high binding potential for Au, they might not be well accessible for adatoms traveling across the surface. One reason could be the presence of structural or electronic barriers around the defects (e.g., Schwoebel barriers) that impede the final diffusion step of an almost thermalized adsorbate into the potential minimum. Such barriers could be induced by the different charge state of V ions in O defects (V^{3+}) versus regular V=O groups (V^{5+}) or by an associated polaronic distortion of the surrounding lattice. The observation of adatoms

sitting next to a defect site, as evident in Figure 5, might be a hint for the presence of diffusion barriers. On the other hand, a missing barrier around V=O defects could explain the occupation of such sites despite of the low Au binding strength.

It should finally be noted that binding energies calculated with the DFT+U approach in ref 23 depend on the choice of the empirical U parameter and are subject to an uncertainty.²⁸ In particular, the calculated preference for Au adsorption to O defects versus regular bridge sites of only 0.2 eV is within the expected accuracy of the method and might even reverse when choosing another computational approach. In this regard, the experimental and theoretical results may partly be reconciled.

4. CONCLUSION

The spatial distribution of Au adatoms on a vanadyl-terminated $V_2O_3(0001)$ surface does not follow a Boltzmann distribution according to the computed binding potential of different regular and defect sites. In fact, the regular V=O bridge position is determined to be the preferred Au adsorption site, although Au binding to O vacancies with an unsaturated V ion should be stronger. This discrepancy suggests that the Au adsorption behavior is not only controlled by thermodynamic aspects but also relies on kinetic limitations that prevent a realization of the energetically favored binding configuration. Although the Au atoms reach the surface with ~ 1000 K, energy dissipation on the V=O-terminated V_2O_3 seems to be efficient enough to restrict transient diffusion of the ad-species to a few dozen steps. As a consequence, the adsorption is dominated by regular sites in the surface, although several defects with higher binding strength are available. Our experiment therefore provides an instructive example for the importance of kinetic aspects when studying adsorption processes away from thermal equilibrium. It demonstrates the sometimes limited comparability between DFT calculations that reveal the energetically preferred binding configuration and the actual situation met in the experiment.

AUTHOR INFORMATION

Corresponding Author

*E-mail: nilius@fhi-berlin.mpg.de.

ACKNOWLEDGMENT

X.L. is grateful for support from the A. v. Humboldt foundation.

REFERENCES

- (1) Freund, H.-J.; Umbach, E., Eds. *Adsorption on Ionic Solids and Thin Films*; Springer: Berlin, 1993.
- (2) Heinrich, V. E.; Cox, P. A. *The Surface Science of Metal Oxides*; University Press: Cambridge, 1994.
- (3) (a) Freund, H.-J. *Faraday Discuss.* **2000**, *114*, 1. (b) Pacchioni, G. *Solid State Sci.* **2000**, *2*, 161.
- (4) (a) Shluger, A. L.; Sushko, P. V.; Kantorovich, L. N. *Phys. Rev. B* **1999**, *59*, 2417. (b) Abbet, S.; Riedo, E.; Brune, H.; Heiz, U.; Ferrari, A.; Giordano, L.; Pacchioni, G. *J. Am. Chem. Soc.* **2001**, *123*, 6172.
- (5) Del Vitto, A.; Pacchioni, G.; Delbecq, F. O.; Sautet, P. *J. Phys. Chem. B* **2005**, *109*, 8040.
- (6) Bikondoa, O.; Pang, C. L.; Ithnin, R.; Muryn, C. A.; Onishi, H.; Thornton, G. *Nat. Mater.* **2006**, *5*, 189.

- (7) Wendt, S.; Schaub, R.; Matthiesen, J.; Vestergaard, E. K.; Wahlstrom, E.; Rasmussen, M. D.; Thostrup, P.; Molina, L. M.; Laegsgaard, E.; Stensgaard, I.; Hammer, B.; Besenbacher, F. *Surf. Sci.* **2005**, *598*, 226.
- (8) Zhao, Y.; Wang, Z.; Cui, X.; Huang, T.; Wang, B.; Luo, Y.; Yang, J.; Hou, J. *J. Am. Chem. Soc.* **2009**, *131*, 7958.
- (9) Diebold, U. *Surf. Sci. Rep.* **2003**, *48*, 53.
- (10) Wöll, C. *Prog. Surf. Sci.* **2007**, *82*, 55.
- (11) Kim, Y. K.; Zhang, Z.; Parkinson, G. S.; Li, S.-C.; Kay, B. D.; Dohnalek, Z. *J. Phys. Chem. C* **2009**, *113*, 20020.
- (12) Surnev, S.; Ramsey, M. G.; Netzer, F. P. *Prog. Surf. Sci.* **2003**, *73*, 117.
- (13) Dupuis, A. C.; Abu Haija, M.; Richter, B.; Kuhlenbeck, H.; Freund, H.-J. *Surf. Sci.* **2003**, *539*, 99.
- (14) Romanyshyn, Y.; Guimond, S.; Kuhlenbeck, H.; Kaya, S.; Blum, R. P.; Niehus, H.; Shaikhutdinov, S.; Simic Milosevic, V.; Nilius, N.; Freund, H.-J.; Ganduglia-Pirovano, M. V.; Fortrie, R.; Döbler, J.; Sauer, J. *Top. Catal.* **2008**, *50*, 106.
- (15) (a) Kresse, G.; Surnev, S.; Schoiswohl, J.; Netzer, F. *Surf. Sci.* **2004**, *555*, 118. (b) Schoiswohl, J.; et al. *Surf. Sci.* **2004**, *555*, 101.
- (16) Schoiswohl, J.; Tzvetkov, G.; Pfuner, F.; Ramsey, M. G.; Surnev, S.; Netzer, F. P. *Phys. Chem. Chem. Phys.* **2006**, *8*, 1614.
- (17) Abu Haija, M.; Guimond, S.; Uhl, A.; Kuhlenbeck, H.; Freund, H.-J. *Surf. Sci.* **2006**, *600*, 1040.
- (18) Göbke, D.; Romanyshyn, Y.; Guimond, S.; Sturm, J. M.; Kuhlenbeck, H.; Döbler, J.; Reinhardt, U.; Ganduglia-Pirovano, M. V.; Sauer, J.; Freund, H.-J. *Angew. Chem., Int. Ed.* **2009**, *48*, 3695.
- (19) Bandara, A.; Abu Haija, M.; Höbel, F.; Kuhlenbeck, H.; Ruppel, G.; Freund, H.-J. *Top. Catal.* **2007**, *46*, 223.
- (20) Abu Haija, M.; Guimond, S.; Uhl, A.; Kuhlenbeck, H.; Freund, H.-J.; Todorova, J. K.; Ganduglia-Pirovano, M. V.; Döbler, J.; Sauer, J. *Surf. Sci.* **2006**, *600*, 1497.
- (21) Sturm, J. M.; Göbke, D.; Kuhlenbeck, H.; Döbler, J.; Reinhardt, U.; Ganduglia-Pirovano, M. V.; Sauer, J.; Freund, H.-J. *Phys. Chem. Chem. Phys.* **2009**, *11*, 3290.
- (22) Nilius, N.; Simic-Milosevic, V. *J. Phys. Chem. C* **2008**, *112*, 10027.
- (23) Nilius, N.; Brázdová, V.; Ganduglia-Pirovano, M.-V.; Simic-Milosevic, V.; Sauer, J.; Freund, H.-J. *New J. Phys.* **2009**, *11*, 093007.
- (24) Rust, H.-P.; Buisset, J.; Schweizer, E. K.; Cramer, L. *Rev. Sci. Instrum.* **1997**, *68*, 129.
- (25) Simic-Milosevic, V.; Nilius, N.; Rust, H.-P.; Freund, H.-J. *Phys. Rev. B* **2008**, *77*, 125112.
- (26) (a) Nilius, N.; Rienks, E.; Rust, H.-P.; Freund, H.-J. *Phys. Rev. Lett.* **2005**, *95*, 066101. (b) Kulawik, M.; Nilius, N.; Freund, H.-J. *Phys. Rev. Lett.* **2006**, *96*, 036103.
- (27) Sterrer, M.; Risse, T.; Martinez Pozzoni, U.; Giordano, L.; Heyde, M.; Rust, H.-P.; Pacchioni, G.; Freund, H.-J. *Phys. Rev. Lett.* **2007**, *98*, 096107.
- (28) Da Silva, J. L. F.; Ganduglia-Pirovano, M. V.; Sauer, J.; Bayer, V.; Kresse, G. *Phys. Rev. B* **2007**, *75*, 045121.